AGU PUBLICATIONS

Geophysical Research Letters

RESEARCH LETTER
10.1002/2016GL069716

Special Section:
Midlatitude Marine Heatwaves: Forcing and Impacts

Key Points:
- Impacts of the 2015-2016 El Nino on the California Current System's physical state are evaluated using model, satellite, and glider data
- Local temperature and density anomalies are much weaker than expected based on tropical sea surface temperature anomalies
- Relatively weak El Nino imprint occurs on backdrop of large multiyear anomalies that may continue to dominate the biological response

Supporting Information:
- Supporting Information S1

Correspondence to:
M. G. Jacox,
mjacox@ucsc.edu

Citation:
Jacox, M. G., E. L. Hazen, K. D. Zaba, D. L. Rudnick, C. A. Edwards, A. M. Moore, and S. J. Bograd (2016), Impacts of the 2015–2016 El Niño on the California Current System: Early assessment and comparison to past events, *Geophys. Res. Lett.*, *43*, 7072–7080, doi:10.1002/2016GL069716.

Received 16 APR 2016
Accepted 13 JUN 2016
Accepted article online 15 JUN 2016
Published online 6 JUL 2016

Impacts of the 2015–2016 El Niño on the California Current System: Early assessment and comparison to past events

Michael G. Jacox[1,2], Elliott L. Hazen[2], Katherine D. Zaba[3], Daniel L. Rudnick[3], Christopher A. Edwards[4], Andrew M. Moore[4], and Steven J. Bograd[2]

[1]Institute of Marine Sciences, University of California, Santa Cruz, California, USA, [2]Environmental Research Division, Southwest Fisheries Science Center, NOAA, Monterey, California, USA, [3]Scripps Institution of Oceanography, La Jolla, California, USA, [4]Ocean Sciences Department, University of California, Santa Cruz, California, USA

Abstract The 2015–2016 El Niño is by some measures one of the strongest on record, comparable to the 1982–1983 and 1997–1998 events that triggered widespread ecosystem change in the northeast Pacific. Here we describe impacts of the 2015–2016 El Niño on the California Current System (CCS) and place them in historical context using a regional ocean model and underwater glider observations. Impacts on the physical state of the CCS are weaker than expected based on tropical sea surface temperature anomalies; temperature and density fields reflect persistence of multiyear anomalies more than El Niño. While we anticipate El Niño-related impacts on spring/summer 2016 productivity to be similarly weak, their combination with preexisting anomalous conditions likely means continued low phytoplankton biomass. This study highlights the need for regional metrics of El Niño's effects and demonstrates the potential to assess these effects before the upwelling season, when altered ecosystem functioning is most apparent.

1. Introduction

The 2015–2016 El Niño continues a string of significant climate events in and around the north Pacific, following an extreme drought that struck California beginning in 2012 [*Swain et al.*, 2014; *Diffenbaugh et al.*, 2015], large-scale anomalous warming of the northeast Pacific beginning in 2013 and reaching record high sea surface temperature (SST) in 2014–2015 [*Bond et al.*, 2015; *Zaba and Rudnick*, 2016], and tropical warming in 2014 that suggested a strong El Niño in winter 2014–2015 [*Ludeschera et al.*, 2014], but failed to develop as expected [*McPhaden*, 2015]. In November 2015, the Niño 3.4 Index indicated the warmest tropical Pacific SST anomalies on record (Figure 1), inviting speculation that the 2015–2016 El Niño could alleviate drought conditions in the western United States and break up the northeast Pacific warm anomaly. In the California Current System (CCS), comparison with past El Niño events of similar magnitude suggests the potential for substantial marine ecosystem impacts. The 1997–1998 El Niño, for example, was implicated in dramatic and widespread changes to the physical, chemical, and biological state of the CCS [e.g., *Kahru and Mitchell*, 2000; *Bograd and Lynn*, 2001; *Chavez et al.*, 2002a, and references therein].

El Niño events can influence the CCS through several mechanisms: (i) remote ocean forcing by poleward coastal wave propagation [*Enfield and Allen*, 1980; *Meyers et al.*, 1998; *Strub and James*, 2002], which depresses the thermocline/nutricline in the CCS [*Huyer and Smith*, 1985; *Chavez et al.*, 2002b; *Frischknecht et al.*, 2015]; (ii) atmospheric teleconnection in which atmospheric Rossby waves excited by tropical convection strengthen the Aleutian Low and displace it to the southeast, reducing (increasing) the strength of upwelling (downwelling) favorable winds along the North American west coast [*Hoskins and Karoly*, 1981; *Alexander et al.*, 2002; *Schwing et al.*, 2002]; and (iii) anomalous advection of warm, saline subtropical water into the CCS from the south [*Bograd and Lynn*, 2001; *Lynn and Bograd*, 2002; *Durazo and Baumgartner*, 2002]. In this paper we focus on (i) and (ii) as they relate to the CCS during the 2015–2016 El Niño. We explore variability in the surface and subsurface temperature and density fields and place these conditions in the context of widespread anomalies of recent years as well as El Niño–Southern Oscillation (ENSO) variability over the past 35 years.

2. Methods

2.1. Data

2.1.1. Temperature

Equatorial Pacific temperature anomalies are characterized using the Niño 3.4 Index (Figure 1a) (http://www.cpc.ncep.noaa.gov/data/indices/), calculated using Extended Reconstructed Sea Surface Temperature v4 with

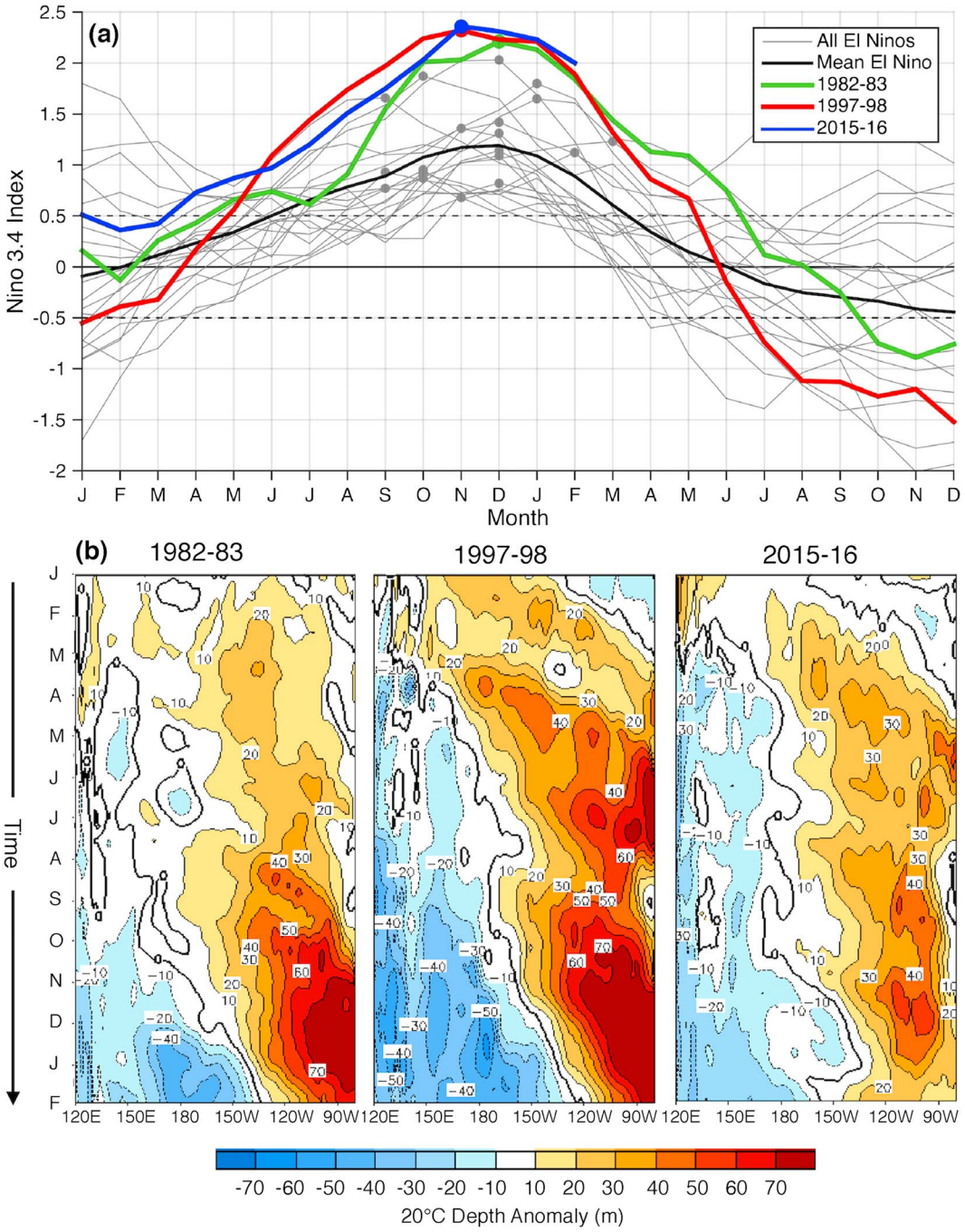

Figure 1. (a) Two-year progression of Niño 3.4 Index for each El Niño since 1950. The circles indicate peak amplitude for each event. The dashed lines mark thresholds used to define El Niño and La Niña events. (b) Hovmöller plots of 20°C isotherm depth anomalies across the equatorial Pacific, averaged from 2°S to 2°N, for January–February of 1982–1983, 1997–1998, and 2015–2016 (adapted from February 2016 CPC ocean briefing; http://origin.cpc.ncep.noaa.gov/products/GODAS/ocean_briefing_gif/).

5 year centered base periods to remove any long-term trends, and 20°C isotherm depth anomalies (Figure 1b), averaged from 2°S to 2°N, from the Global Ocean Data Assimilation System. We compare SST anomalies in the CCS during past strong El Niños (Figure 2) using NOAA's 0.25° optimum interpolation SST product (OISST.v2) [*Reynolds et al.*, 2007].

2.1.2. Chlorophyll

Surface chlorophyll estimates for 1998–2016 are from the merged 4 km resolution CCS data set described by *Kahru et al.* [2012, 2015], which utilizes >12,000 in situ measurements to regionally optimize and combine

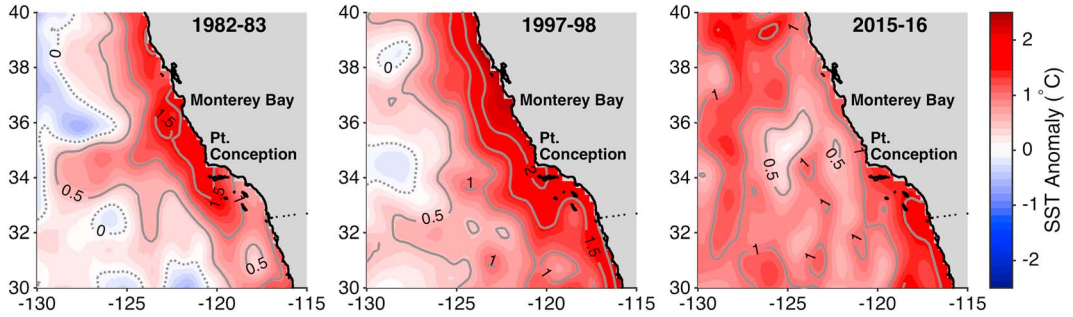

Figure 2. December–February mean SST anomalies for the winters of 1982–1983, 1997–1998, and 2015–2016. Anomalies are calculated using NOAA's 0.25° OISST product with a 1981–2015 base period.

surface chlorophyll algorithms for five satellite ocean color sensors (Ocean Color and Temperature Scanner, Sea-Viewing Wide Field-of-View Sensor, Medium-Resolution Imaging Spectrometer, Moderate Resolution Imaging Spectroradiometer A, and Visible Infrared Imaging Radiometer Suite).

2.1.3. Wind

Wind stress estimates are provided by the European Centre for Medium-Range Weather Forecasts (ECMWF) Interim reanalysis [*Dee et al.*, 2011]. Monthly means of daily northward and eastward surface wind stress were rotated parallel to the local coastline orientation to obtain alongshore wind stress.

2.1.4. Underwater Gliders

Since late 2006, the California Underwater Glider Network (CUGN) has used Spray gliders [*Sherman et al.*, 2001; *Rudnick et al.*, 2004] to occupy lines 66.7, 80, and 90 of the California Cooperative Oceanic Fisheries Investigations sampling grid (Figure 3). Each glider line extends 350–500 km offshore and takes 2–3 weeks to complete. Gliders obtain vertical profiles from the surface to 500 m depth at a horizontal spacing of ~3 km and vertical sampling resolution of ~1 m. As in *Zaba and Rudnick* [2016], we objectively map glider data to

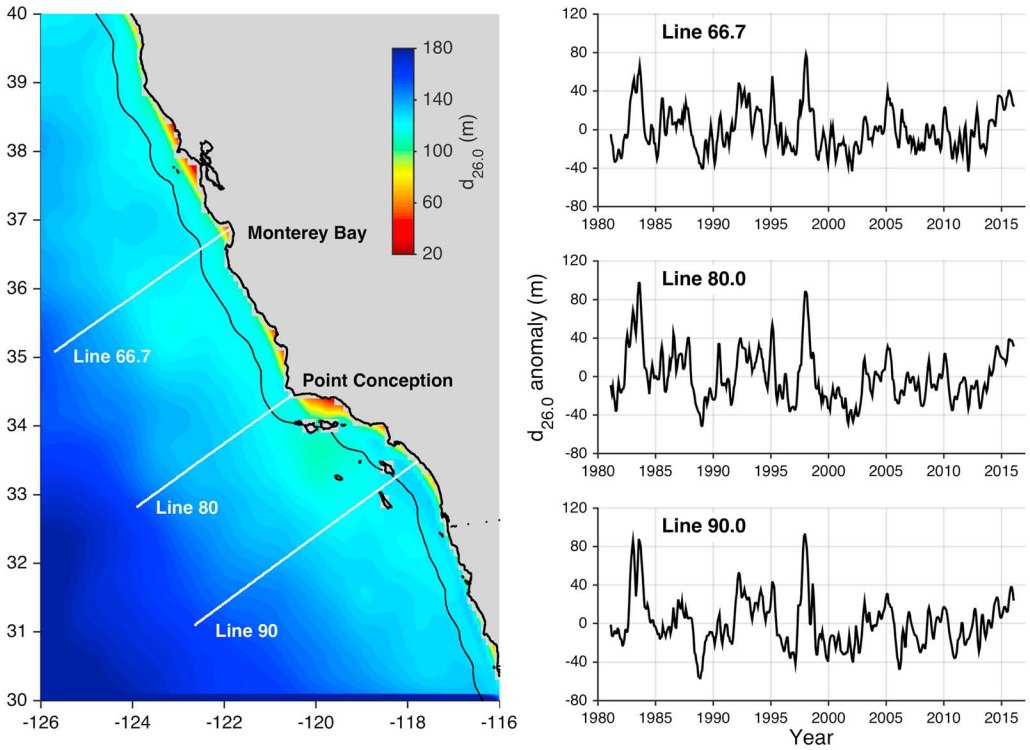

Figure 3. (left) December–February mean depth of the 26.0 kg m^{-3} isopycnal ($d_{26.0}$), computed from the ROMS reanalysis for the years 1981–2010. The white lines are nominal positions of glider tracks, and a black contour marks 50 km from shore. (right) January 1981 to February 2016 time series of $d_{26.0}$ anomalies from the merged model-glider data.

three-dimensional grids [*Bretherton et al.*, 1976] with horizontal, vertical, and temporal resolutions of 5 km, 10 m, and 10 days, respectively. Horizontal and temporal decorrelation scales of 30 km and 60 days, respectively, are used in the mapping algorithm to filter out high-frequency variability [*Rudnick and Cole*, 2011].

2.2. Ocean Model

A 30 year (1981–2010) regional ocean reanalysis provides historical context for impacts of ENSO variability on the CCS. This reanalysis uses the Regional Ocean Modeling System (ROMS) with 4-Dimensional Variational (4D-Var) data assimilation and is described in detail elsewhere [*Neveu et al.*, 2016]. The model domain covers 30–48°N and 134–115.5°W with 1/10° horizontal resolution and 42 vertical levels. Surface forcing derives from a combination of the ECMWF 40 year (ERA-40) [*Uppala et al.*, 2005] and ERA Interim reanalyses and Cross-Calibrated Multi Platform winds [*Atlas et al.*, 2011]. Lateral boundary conditions are provided by the Simple Ocean Data Assimilation reanalysis [*Carton and Giese*, 2008]. Assimilated data include satellite SST and sea surface height, and in situ hydrographic data from version 2a of the quality-controlled ENSEMBLES database maintained by the UK Met Office [*Ingleby and Huddleston*, 2007]. This reanalysis has been used to investigate physical and biogeochemical dynamics off the U.S. west coast, including ENSO-driven variability [*Jacox et al.*, 2014, 2015a]. The same model, configured without data assimilation, was used to quantify individual influences of ENSO-related changes in surface wind, heat flux, and remote ocean forcing (imparted through the lateral boundaries) on upwelled nitrate supply in the CCS [*Jacox et al.*, 2015b].

2.3. Merging Model and Glider Data

Output from the ROMS reanalysis and data from the CUGN cover the periods 1981–2010 and 2007 to present, respectively. Here we merge these two data sets to develop self-consistent time series for 1981 to present, providing historical context for the conditions accompanying the 2015–2016 El Niño. We do not attempt to fully merge the modeled and glider-based ocean state estimates. Rather, we focus on a key derived variable, the depth of the 26.0 kg m^{-3} isopycnal ($d_{26.0}$), which is closely tied to nutrient supply and resultant productivity, and can be modulated by local upwelling [*Lynn et al.*, 2003], remote (e.g., ENSO-related) forcing [*Jacox et al.*, 2015a], and local forcing by air/sea heat flux and wind stress [*Zaba and Rudnick*, 2016]. Note that while $d_{26.0}$ is sometimes used as a proxy for pycnocline depth, the two can be decoupled [*Kim and Miller*, 2007]. We find that $d_{26.0}$ is more closely coupled to surface chlorophyll anomalies in the central/southern CCS (not shown), so we retain it for our analysis. For each of the three glider lines, we compute monthly mean $d_{26.0}$ and average across a 50 km coastal band, chosen to reflect the region of greatest physical influence by coastal waves and anomalous upwelling associated with ENSO. Model-based estimates of $d_{26.0}$ are similarly averaged in time and space, using grid cells that overlap glider tracks. Model and glider-based estimates of $d_{26.0}$ are shown in Figure S1 in the supporting information for the 4 year period (2007–2010) in which they overlap. While model estimates of $d_{26.0}$ are strongly correlated with glider estimates ($r = 0.75$–0.87; Figure S2), they are generally too deep and underestimate the observed variance, consistent with known warm biases and underestimation of salinity variability at typical depths of $d_{26.0}$ [*Neveu et al.*, 2016]. We therefore use the 2007–2010 data to adjust model estimates of $d_{26.0}$ on each line such that they match the mean and variance of glider estimates for the overlapping period (Figure S1). The corrected model estimates are then combined with glider estimates to produce self-consistent time series of $d_{26.0}$ extending from 1981 to early 2016.

2.4. Confidence Intervals for Chlorophyll Regressions

For regressions of chlorophyll anomalies against subsurface density anomalies (sections 5 and 6), we use a bootstrap analysis to calculate 95% confidence intervals. We perform linear regressions 1000 times, each time randomly resampling the data with replacement. Confidence intervals for regression lines and correlation coefficients are ±1.96 SE, where $\mathrm{SE} = \sigma/\sqrt{n}$, σ is the standard deviation of the bootstrapped regressions and n is the number of data points.

3. Tropical Pacific Temperature Anomalies

While peak tropical SST anomalies (as measured by the Niño 3.4 Index) were nearly identical in the 1982–1983, 1997–1998, and 2015–2016 El Niños (~2.3°C), the temporal evolution of SST anomalies differed considerably between events (Figure 1). The 1997–1998 El Niño was notable not only for its maximum magnitude but also for dramatic transitions out of the cool conditions of 1996–1997 and into the strong 1998–1999 La Niña. In contrast, the tropical Pacific was already anomalously warm prior to the ramp-up of the 2015–2016 El Niño,

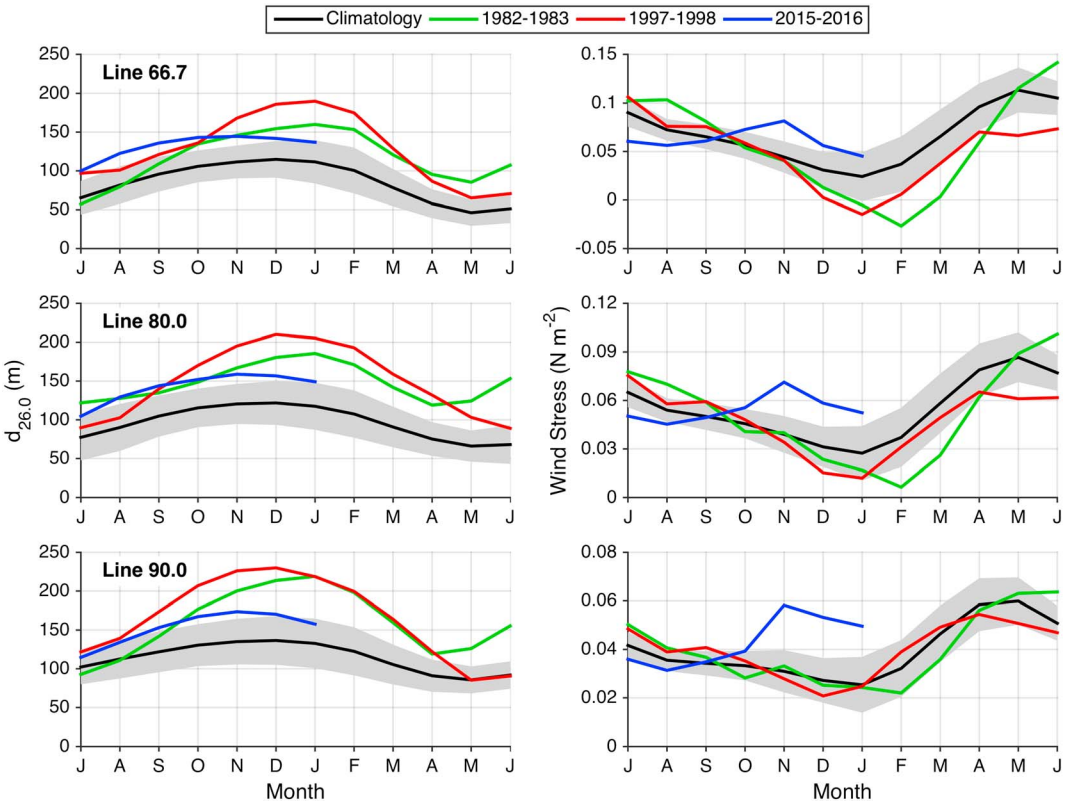

Figure 4. Annual (July–June) evolution of (left) $d_{26.0}$ and (right) alongshore wind stress for 1982–1983, 1997–1998, and 2015–2016, as compared to the 1981–2015 climatology. Alongshore wind stress was calculated 50 km from shore and averaged over 3° of latitude surrounding each line (35–38°N, 33–36°N, and 32–35°N for lines 66.7, 80, and 90, respectively). Positive wind stress is equatorward (upwelling favorable). All time series are smoothed with a 3 month running mean. Gray shading marks ±1 standard deviation of monthly means.

owing to an aborted El Niño the year prior [*McPhaden*, 2015]. The net warming in the year preceding the 1997 peak (i.e., November 1996 to November 1997) was a full degree higher than in the year preceding the 2015 peak (2.7°C versus 1.6°C), while the year preceding the 1982 peak saw a 2.3°C increase.

The more rapid physical oceanographic change during past strong El Niños than during the 2015–2016 event was also reflected in the subsurface temperature field, specifically the 20°C isotherm depth (d_{20C}). The 1982–1983 and 1997–1998 El Niños were characterized by eastward propagation of d_{20C} anomalies and east-west dipoles with eastern equatorial d_{20C} anomalies >60 m persisting from October through February (Figure 1b). In 2015–2016, however, a much weaker subsurface signal was observed. Eastward propagation of several Kelvin waves, generated by westerly wind bursts (Climate Prediction Center (CPC) briefing, January 2016; http://origin.cpc.ncep.noaa.gov/products/GODAS/ocean_briefing_gif/), is evident in d_{20C} anomalies. However, in contrast to 1982–1983 and 1997–1998, 2015–2016 was characterized by a relatively weak east-west dipole that appears to reflect persistence of existing anomalies rather than a building El Niño. Together, these observations indicate a partial decoupling of the surface and subsurface temperature fields between the strongest El Niños; while in each event some degree of warming is visible throughout the upper water column in the eastern tropical Pacific, similar surface warming does not necessarily translate to similar subsurface anomalies.

4. Development of the 2015–2016 El Niño in the CCS Relative to Past Events

In the CCS, physical oceanographic anomalies during the 2015–2016 El Niño departed from those seen during the strongest historical events, mirroring the previously described tropical subsurface dynamics. During the winters of 1982–1983 and 1997–1998, CCS SST anomalies were greatest near shore (Figure 2), consistent with a deep thermocline and anomalously weak upwelling, and marked cross-shore SST gradients extended hundreds of kilometers offshore. While positive SST anomalies were also observed near shore during the 2015–2016 El Niño,

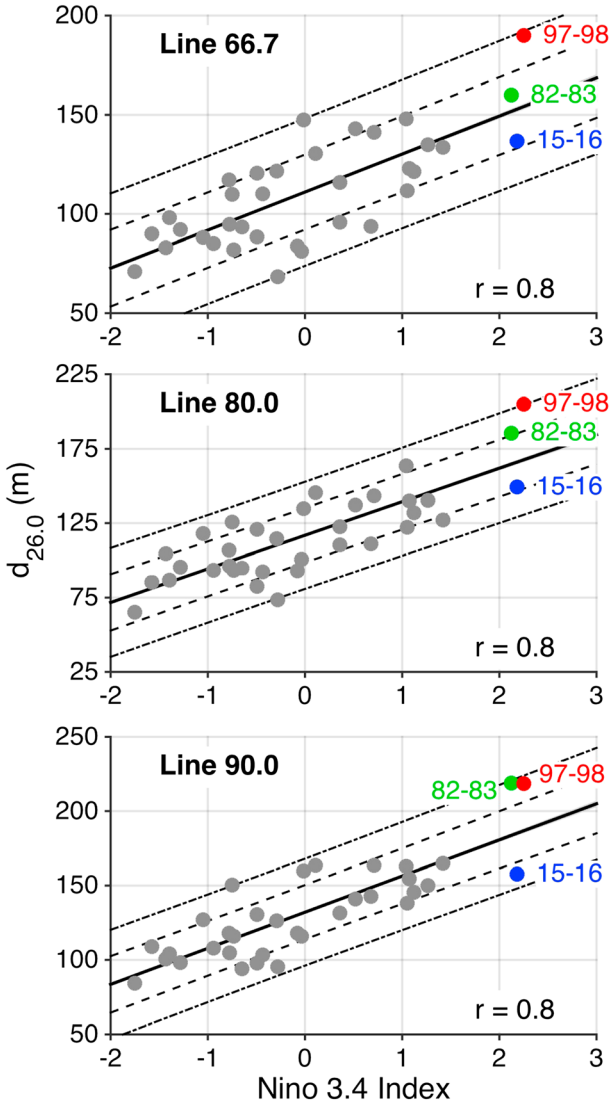

Figure 5. December–February mean $d_{26.0}$ (from merged model-glider data) plotted against November–January mean Niño 3.4 anomalies for each winter from 1981–1982 to 2015–2016. Isopycnal depths are averaged within 50 km of shore. The solid lines are linear fits to the data; the dashed and dash-dotted lines are ±1 and ±2 standard deviations from the linear fit.

particularly south of Point Conception, cross-shore gradients were much less pronounced and the broad-scale temperature structure appears to be more consistent with ongoing decay of preexisting northeast Pacific warm anomalies [*Bond et al.*, 2015; *Zaba and Rudnick*, 2016] than with a warming signature of El Niño.

The subsurface tells a similar story; anomalies in the 26.0 kg m^{-3} isopycnal depth ($d_{26.0}$) were already established by mid-2014 [*Zaba and Rudnick*, 2016] and remained nearly constant through late 2015 into 2016 (compare 2015–2016 (blue) to climatology (black) in Figure 4, left column). In contrast, past strong El Niños were characterized by a dramatic deepening of $d_{26.0}$ in the latter half of the year and peak anomalies in December/January (Figure 4), consistent with documented lags of 1–2 months from the tropics to the CCS [e.g., *Jacox et al.*, 2015a]. While our 35 year time series show considerable correlation between the Niño 3.4 Index and wintertime $d_{26.0}$ off central/southern California ($r \approx 0.8$; Figure 5), the three strongest El Niños highlight important variability in this relationship. In 1982–1983, $d_{26.0}$ ranged from ~0.5 to 2 standard deviations (σ) deeper than that predicted by Niño 3.4, and $d_{26.0}$ in 1997–1998 was ~2σ deeper than that predicted by Niño 3.4. In contrast, $d_{26.0}$ in 2015–2016 was ~1σ shallower than that predicted by the Niño 3.4 anomaly (Figure 5). The observed CCS $d_{26.0}$ anomalies are consistent with a relatively weak oceanic teleconnection from the tropics in 2015–2016.

Surface winds in the winter of 2015–2016 were similarly uncharacteristic of El Niño. During 1982–1983 and 1997–1998, alongshore winds were near their climatological means off southern California (line 90) and anomalously weak or poleward from midwinter through spring off central California (Figure 4). Increasing upwelling favorable winds from July to November 2015, especially off southern California, ran counter to climatological patterns and past El Niños. Relatively strong equatorward winds in November–January 2015 likely contributed to a reduction in $d_{26.0}$ anomalies during those months (Figure 4). The divergence of regional wind patterns in 2015–2016 from those seen in 1982–1983 and 1997–1998 suggests that as for $d_{26.0}$, predictability of CCS conditions based on tropical SST anomalies is limited for any individual El Niño event.

5. Impacts on Phytoplankton in the Central and Southern CCS

The 1982–1983 and 1997–1998 El Niños were both followed by sharp reductions in spring/summer phytoplankton biomass off the California coast [*Fiedler*, 1984; *Kahru and Mitchell*, 2000]. These reductions were

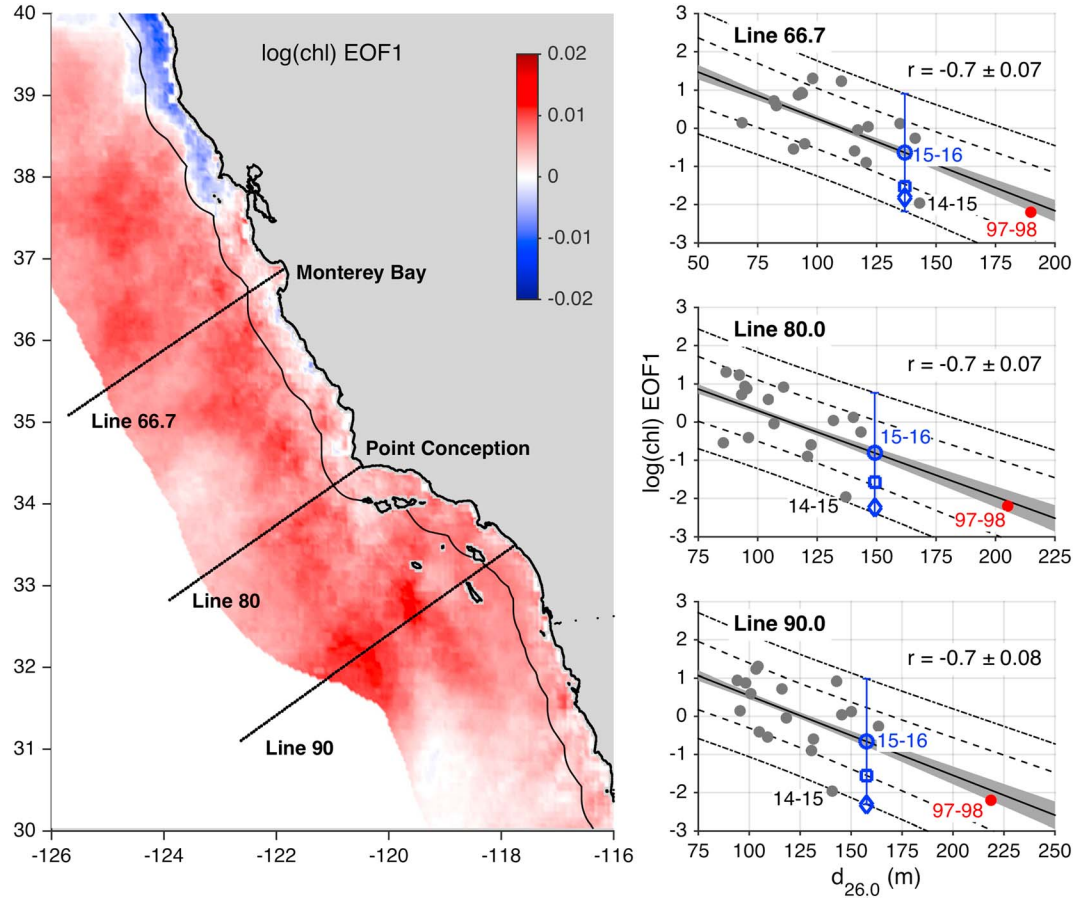

Figure 6. (left) Leading EOF of surface chlorophyll, 30–40°N and 0–300 km from shore, computed from April to July averages of log-transformed chlorophyll for 1998–2015. EOF1 captures 32% of the observed variance. (right) Amplitude of EOF1 time series plotted against December–February mean $d_{26.0}$, averaged within 50 km of shore (e.g., "1997–1998" is log(chl) EOF1 for April–July 1998 plotted against $d_{26.0}$ for December 1997 to February 1998). The solid black lines are linear fits to the data; the dashed and dash-dotted lines are ±1 and ±2 standard deviations about the linear fit. The 95% confidence intervals for linear regressions (gray shading) and correlation coefficients were determined from a bootstrap analysis (see Methods section). Three estimates for spring/summer 2016 chlorophyll (open blue markers) are estimated from the observed winter 2015–2016 $d_{26.0}$. They assume (i) a return to the regression line (circle), (ii) a repeat of spring/summer 2015 anomalies (diamond, ~2σ below the regression line), and (iii) persistence of March 2016 anomalies (square, ~1σ below the regression line; see Figure S3).

attributed to weak upwelling and/or a deep pycnocline/nutricline, each of which decreases nutrient supply to the surface mixed layer. Here we explore the relationship between winter (December–February) $d_{26.0}$ variability and biological impacts the following spring using an empirical orthogonal function (EOF) decomposition of the surface chlorophyll field. Specifically, we calculate EOFs from 18 years (1998–2015) of April–July mean log-transformed surface chlorophyll in a spatial domain spanning 30°N–40°N and 0–300 km from shore. The first EOF explains 32% of the observed variance and captures broad-scale inter-annual variability in spring/summer chlorophyll concentrations south of San Francisco Bay (~38°N; Figure 6). EOF1 is negatively correlated with wintertime $d_{26.0}$ on all three glider lines ($r = -0.7 \pm 0.07$), suggesting that the physical ocean state in winter is a useful leading indicator of upwelling season productivity. Exclusion of 1997–1998 from the regressions in Figure 6 lowers the strength of correlations ($r = -0.5 \pm 0.08$) but does not appreciably alter the regression line. Interestingly, the correlation between EOF1 and the Niño 3.4 Index is significantly weaker ($r = -0.5 \pm 0.07$ with 1997–1998, $r = -0.3 \pm 0.08$ without), further demonstrating the limitations of projecting El Niño impacts on the CCS from tropical SST anomalies alone. Note that the lower modes of chlorophyll variability (not shown; EOF2, 11% explained variance; EOF3, 10% explained variance) describe spatially heterogeneous fluctuations that are not strongly correlated with $d_{26.0}$ ($r = 0.1$–0.3) or Niño 3.4 ($r = 0.1$).

6. Predicting Chlorophyll Anomalies for Spring/Summer 2016

Based solely on $d_{26.0}$ in winter 2015–2016 and the linear regressions in Figure 6, spring/summer 2016 chlorophyll anomalies off central and southern California should be negative, but of far smaller magnitude than those seen in 1998. However, unprecedented warming of the northeast Pacific in the past 2 years was accompanied by biological changes in the CCS including strongly negative chlorophyll anomalies (Figure 6), anomalously deep chlorophyll maxima [*Zaba and Rudnick*, 2016], and dramatic impacts on species abundance and distributions throughout the marine food web [*Bond et al*., 2015; *Peterson et al*., 2016]. Thus, two alternate hypotheses for spring/summer 2016 are (i) the background ocean state returns to something near the climatological mean, and surface chlorophyll anomalies are much smaller than they were in 1998, consistent with historical physical-biological relationships (blue circle in Figure 6), and (ii) the impact of preexisting anomalous conditions persists, and chlorophyll concentrations remain suppressed at levels comparable to those observed in 1998 and 2015 (blue diamond in Figure 6). At the time of writing, the latest available chlorophyll data (March 2016; Figure S3) suggest something between (i) and (ii), with 2016 values falling ~1σ below the regression line (blue square in Figure 6), behind only 1998 and 2015 in terms of low chlorophyll anomalies in the past two decades.

7. Conclusion

While tropical Pacific SST anomalies reached record highs in late 2015, they were not accompanied by strong equatorial Kelvin wave generation or weakened upwelling-favorable winds in the central/southern CCS. The response in the subsurface density field off California was accordingly weak, especially when compared to the 1982–1983 and 1997–1998 El Niños. We therefore expect the impacts of the 2015–2016 El Niño on primary production in the CCS to be less than in the 1982–1983 or 1997–1998 El Niños. However, it is important to note that a highly anomalous ocean state in place prior to the 2015–2016 El Niño is likely to contribute to continued low chlorophyll biomass.

El Niños are now understood to be highly diverse in their expressions [*Capotondi et al*., 2015], and the disparity in CCS responses to El Niño events of similar magnitude (based on widely used indices) highlights the need for more holistic measures of ENSO events and/or regional metrics of their effects. We have shown one example of the latter ($d_{26.0}$), which is influenced by ENSO variability but improves predictions of biological impacts in the CCS relative to the Niño 3.4 Index. This study also demonstrates a capability to assess in near real time the regional impacts of an ongoing El Niño using the best available data from ocean models, satellites, and autonomous platforms.

Acknowledgments

This work was supported by funding from NSF grant OCE1061434 and NOAA's Integrated Ecosystem Assessment program. The California Underwater Glider Network (CUGN) is supported by the NOAA Climate Observations Division (NA10OAR4320156) and the Southern California Coastal Ocean Observing System (NA11NOS0120029). Model output from the ROMS historical reanalysis can be obtained from oceanmodeling.ucsc.edu. Data from the CUGN can be obtained via NOAA ERDDAP (http://coastwatch.pfeg.noaa.gov/erddap/index.html). Niño 3.4 indices and 20°C isotherm depths are available from the CPC (http://www.cpc.ncep.noaa.gov/data/indices/ and http://www.cpc.ncep.noaa.gov/products/GODAS/pentad.shtml, respectively). We thank Mati Kahru for providing the CCS chlorophyll product used herein (available at http://spg.ucsd.edu/Satellite_Data/CC4km/CC4km.htm). We also thank Nate Mantua and two anonymous reviewers for their helpful comments on an earlier version of the manuscript.

References

Alexander, M. A., I. Bladé, M. Newman, J. R. Lanzante, N. C. Lau, and J. D. Scott (2002), The atmospheric bridge: The influence of ENSO teleconnections on air-sea interaction over the global oceans, *J. Clim.*, *15*(16), 2205–2231.

Atlas, R., R. N. Hoffman, J. Ardizzone, S. M. Leidner, J. C. Jusem, D. K. Smith, and D. Gombos (2011), A cross-calibrated, multiplatform ocean surface wind velocity product for meteorological and oceanographic applications, *Bull. Am. Meteorol. Soc.*, *92*, 157–174, doi:10.1175/2010BAMS2946.1.

Bograd, S. J., and R. J. Lynn (2001), Physical-biological coupling in the California Current during the 1997–1999 El Niño-La Niña cycle, *Geophys. Res. Lett.*, *28*, 275–278, doi:10.1029/2000GL012047.

Bond, N. A., M. F. Cronin, H. Freeland, and N. Mantua (2015), Causes and impacts of the 2014 warm anomaly in the NE Pacific, *Geophys. Res. Lett.*, *42*, 3414–3420, doi:10.1002/2015GL063306.

Bretherton, F. P., R. E. Davis, and C. B. Fandry (1976), Technique for objective analysis and design of oceanographic experiments applied to MODE-73, *Deep Sea Res.*, *23*(7), 559–582, doi:10.1016/0011-7471(76)90001-2.

Capotondi, A., et al. (2015), Understanding ENSO diversity, *Bull. Am. Meteorol. Soc.*, *96*(6), 921–938.

Carton, J. A., and B. S. Giese (2008), A reanalysis of ocean climate using Simple Ocean Data Assimilation (SODA), *Mon. Weather Rev.*, *136*, 2999–3017.

Chavez, F. P., C. A. Collins, A. Huyer, and D. L. Mackas (2002a), El Niño along the west coast of North America, *Prog. Oceanogr.*, *54*(1), 1–5.

Chavez, F., J. Pennington, C. Castro, J. Ryan, R. Michisaki, B. Schlining, P. Walz, K. Buck, A. McFadyen, and C. Collins (2002b), Biological and chemical consequences of the 1997–1998 El Niño in central California waters, *Prog. Oceanogr.*, *54*(1-4), 205–232, doi:10.1016/S0079-6611(02)00050-2.

Dee, D. P., et al. (2011), The ERA-Interim reanalysis: Configuration and performance of the data assimilation system, *Q. J. R. Meteorol. Soc.*, *137*, 553–597.

Diffenbaugh, N. S., D. L. Swain, and D. Touma (2015), Anthropogenic warming has increased drought risk in California, *Proc. Natl. Acad. Sci. U.S.A.*, *112*(13), 3931–3936.

Durazo, R., and T. Baumgartner (2002), Evolution of oceanographic conditions off Baja California: 1997–1999, *Prog. Oceanogr.*, *54*(1–4), 7–31, doi:10.1016/S0079-6611(02)00041-1.

Enfield, D., and J. Allen (1980), On the structure and dynamics of monthly mean sea-level anomalies along the Pacific coast of North and South-America, *J. Phys. Oceanogr.*, *10*(4), 557–578, doi:10.1175/1520-0485(1980)0102.0.CO;2.

Fiedler, P. C. (1984), Satellite observations of the 1982–1983 El Niño along the U.S. Pacific coast, *Science*, *224*(4654), 1251–1254.

Frischknecht, M., M. Münnich, and N. Gruber (2015), Remote versus local influence of ENSO on the California Current System, *J. Geophys. Res. Oceans*, *120*, 1353–1374, doi:10.1002/2014JC010531.

Hoskins, B. J., and D. J. Karoly (1981), The steady linear response of a spherical atmosphere to thermal and orographic forcing, *J. Atmos. Sci.*, *38*(6), 1179–1196.
Huyer, A., and R. L. Smith (1985), The signature of El Niño off Oregon, 1982–1983, *J. Geophys. Res.*, *90*, 7133–7142, doi:10.1029/JC090iC04p07133.
Ingleby, B., and M. Huddleston (2007), Quality control of ocean temperature and salinity profiles - Historical and real-time data, *J. Mar. Syst.*, *65*, 158–175.
Jacox, M. G., A. M. Moore, C. A. Edwards, and J. Fiechter (2014), Spatially resolved upwelling in the California Current System and its connections to climate variability, *Geophys. Res. Lett.*, *41*, 3189–3196, doi:10.1002/2014GL059589.
Jacox, M. G., J. Fiechter, A. M. Moore, and C. A. Edwards (2015a), ENSO and the California Current coastal upwelling response, *J. Geophys. Res. Oceans*, *120*, 1691–1702, doi:10.1002/2014JC010650.
Jacox, M. G., S. J. Bograd, E. L. Hazen, and J. Fiechter (2015b), Sensitivity of the California Current nutrient supply to wind, heat, and remote ocean forcing, *Geophys. Res. Lett.*, *42*, 5950–5957, doi:10.1002/2015GL065147.
Kahru, M., and B. G. Mitchell (2000), Influence of the 1997–1998 El Nino on the surface chlorophyll in the California Current, *Geophys. Res. Lett.*, *27*(18), 2937–2940, doi:10.1029/2000GL011486.
Kahru, M., R. M. Kudela, M. Manzano-Sarabia, and B. G. Mitchell (2012), Trends in the surface chlorophyll of the California Current: Merging data from multiple ocean color satellites, *Deep Sea Res., Part II*, *77-80*, 89–98.
Kahru, M., R. M. Kudela, C. R. Anderson, and B. G. Mitchell (2015), Optimized merger of ocean color algorithms, *IEEE Geosci. Remote Sens. Lett.*, *12*(11), 2282–2285.
Kim, H. J., and A. J. Miller (2007), Did the thermocline deepen in the California Current after the 1976/1977 climate regime shift?, *J. Phys. Oceanogr.*, *37*, 1733–1739.
Ludeschera, J., A. Gozolchianib, M. I. Bogacheva, A. Bundea, S. Havlin, and H. J. Schellnhuberd (2014), Very early warning of next El Niño, *Proc. Natl. Acad. Sci. U.S.A.*, *111*(6), 2064–2066, doi:10.1073/pnas.1323058111.
Lynn, R. J., and S. J. Bograd (2002), Dynamic evolution of the 1997–1999 El Niño-La Niña cycle in the southern California Current System, *Prog. Oceanogr.*, *54*, 59–75.
Lynn, R. J., S. J. Bograd, T. K. Chereskin, and A. Huyer (2003), Seasonal renewal of the California Current: The spring transition off California, *J. Geophys. Res.*, *108*(C8), 3279, doi:10.1029/2003JC001787.
McPhaden, M. J. (2015), Playing hide and seek with El Niño, *Nat. Clim. Change*, *5*, 791–795.
Meyers, S. D., A. Melsom, G. T. Mitchum, and J. J. O'Brien (1998), Detection of the fast Kelvin wave teleconnection due to El Niño-Southern Oscillation, *J. Geophys. Res.*, *103*(C12), 27,655–27,663, doi:10.1029/98JC02402.
Neveu, E., A. M. Moore, C. A. Edwards, J. Fiechter, P. Drake, W. J. Crawford, M. G. Jacox, and E. Nuss (2016), An historical analysis of the California Current circulation using ROMS 4D-Var. Part I: System configuration and diagnostics, *Ocean Modell*, *99*, 133–151, doi:10.1016/j.ocemod.2015.11.012.
Peterson, W., N. Bond, and M. Robert (2016), The Blob (Part Three): Going, going, gone?, *PICES Press*, *24*(1), 46–48.
Reynolds, R. W., T. M. Smith, C. Liu, D. B. Chelton, K. S. Casey, and M. G. Schlax (2007), Daily high-resolution-blended analyses for sea surface temperature, *J. Clim.*, *20*, 5473–5496.
Rudnick, D. L., and S. T. Cole (2011), On sampling the ocean using underwater gliders, *J. Geophys. Res.*, *116*, C08010, doi:10.1029/2010JC006849.
Rudnick, D. L., R. E. Davis, C. C. Eriksen, D. M. Fratantoni, and M. J. Perry (2004), Underwater gliders for ocean research, *Mar. Technol. Soc. J.*, *38*(2), 73–84.
Schwing, F., T. Murphree, L. DeWitt, and P. Green (2002), The evolution of oceanic and atmospheric anomalies in the northeast Pacific during the El Niño and La Niña events of 1995–2001, *Prog. Oceanogr.*, *54*(1–4), 459–491, doi:10.1016/S0079-6611(02)00064-2.
Sherman, J., R. E. Davis, W. B. Owens, and J. Valdes (2001), The autonomous underwater glider "Spray", *IEEE J. Oceanic Eng.*, *26*(4), 437–446.
Strub, P., and C. James (2002), The 1997–1998 oceanic El Niño signal along the southeast and northeast Pacific boundaries—An altimetric view, *Prog. Oceanogr.*, *54*(1–4), 439–458, doi:10.1016/S0079-6611(02)00063-0.
Swain, D. L., M. Tsiang, M. Haugen, D. Singh, A. Charland, B. Rajaratnam, and N. S. Diffenbaugh (2014), The extraordinary California drought of 2013/2014: Character, context, and the role of climate change, *Bull. Am. Meteorol. Soc.*, *95*(9), S3.
Uppala, S. M., et al. (2005), The ERA-40 re-analysis, *Q. J. R. Meteorol. Soc.*, *131*, 2961–3012.
Zaba, K. D., and D. L. Rudnick (2016), The 2014–2015 warming anomaly in the Southern California Current System observed by underwater gliders, *Geophys. Res. Lett.*, *43*, 1241–1248, doi:10.1002/2015GL067550.